TIME-DOMAIN ANALYSIS OF 3-PHASE ARC FLASH HAZARD

R. Wilkins, M. Allison and **M. Lang**

Ferraz Shawmut, 374 Merrimac St, Newburyport, MA 01950, USA
bobwilkins@clara.co.uk , malcolm.allison@ferrazshawmut.com , mike.lang@ferrazshawmut.com

Abstract: Conventional arc flash hazard calculators use simple formulae to calculate the flash protection boundary and the incident energy density. A new method is described which models the circuit response and the operation of current-limiting fuses in the time domain, and the radiation-focusing effect of the equipment enclosure. The fault arcs are represented by a semi-empirical *v/i* model.

Keywords: arc flash hazard, current-limiting fuses

1. Introduction

The 2002 edition of the NEC requires equipment, on which work may be required to be done when energized, to be labelled, warning of arc flash hazard [1-3]. The 2003 edition of NFPA 70E requires a flash hazard analysis to be done before a person can work near to energized equipment, and to determine the type of protective clothing needed [2].

There are several different methods in use at present to calculate the flash boundary distance and incident energy upon a worker [2,4-7], and the new IEEE standard 1584 proposes a formula based on a statistical fit to test data obtained in several high-power test laboratories in North America [8].

In this paper a time-domain analysis method is presented, which can be used as an arc flash calculator, and which also allows current-limitation by fuses and other effects to be studied.

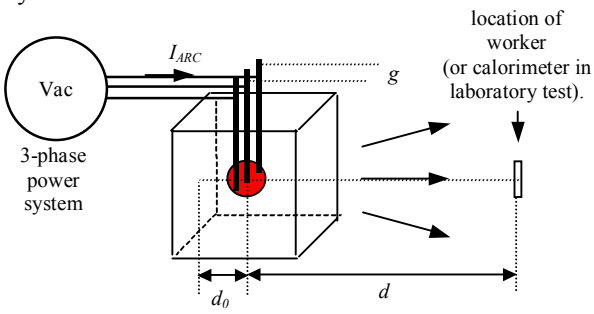

Fig. 1: Arc flash in an open box

Fig. 1 shows a schematic representation of an arc flash hazard incident. In laboratory tests the arcs are initiated by fine trigger fuse wires. High-current arcs which are not restricted move, due to magnetic forces, so as to increase the area of the circuit loop. For the geometry shown this causes the arcs to be driven downwards and to burn at the electrode-busbar tips, to form what is commonly referred to as a 3-phase "arcing fireball".

However the behaviour of the 3-phase free-burning arcing fault in equipment is chaotic, involving rapid and irregular changes in arc geometry due to thermal buoyancy and electromagnetic forces, arc extinction, plasma jets, sudden shortening due to restriking and reconnection across electrodes or plasma parts, and many other effects.

2. Time domain model

The given quantities are the network data (voltage, bolted-fault current, frequency, X/R ratio) and the equipment dimensions (bus electrode gap and location, box dimensions). It is required to calculate the arcing current (so that the operating time of protective devices can be found), and then the incident energy density E_i due to thermal radiation at a distance d from the arcing fireball.

Most conventional arc flash hazard calculators use a least-squares best-fit to the test data to give simple formulae for I_{ARC} and E_i in terms of the input data. Although the fault arc behaviour is difficult to model, the behaviour of the other parts of the system (electrical circuit, current-limiting fuse, thermal radiation) are well-known. These parts can be modelled accurately in the time-domain, reducing the area of uncertainty to that of the arcing fireball itself.

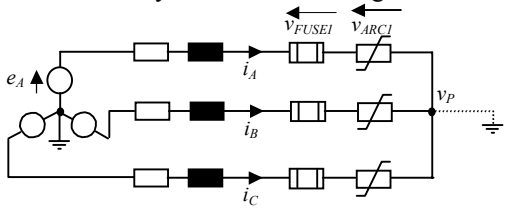

Fig. 2: Circuit model

Fig. 2 shows the circuit model, which includes a set of 3 current-limiting fuses in series with the arcing fault. The arcing fault is initially modelled as a set of fine trigger fuse wires with a fixed melting I^2t, and then the subsequent arcing fireball is modelled as a star-connected set of non-linear resistances. For ungrounded faults the sum of the phase currents is zero, which enables the potential v_P to be calculated. The transient circuit current can then be found by numerical solution of the circuit differential equations :

$$\begin{aligned}\frac{di_A}{dt} &= \frac{e_A - Ri_A - v_{FUSE1} - v_{ARC1} - v_P}{L} \\ \frac{di_B}{dt} &= \frac{e_B - Ri_B - v_{FUSE2} - v_{ARC2} - v_P}{L} \\ \frac{di_C}{dt} &= \frac{e_C - Ri_C - v_{FUSE3} - v_{ARC3} - v_P}{L}\end{aligned} \qquad (1)$$

$v_P = 0$ if the star point is grounded, otherwise

(a) if all fuses are intact

$$v_P = -(v_{FUSE1} + v_{FUSE2} + v_{FUSE3} + v_{ARC1} + v_{ARC2} + v_{ARC3})/3$$

(b) after 1st fuse has cleared (say in phase *a*)

$$v_P = (e_B + e_C - v_{FUSE2} - v_{FUSE3} - v_{ARC2} - v_{ARC3})/2$$

Cyclically similar expressions may be written if phase *b* or phase *c* clears first [9]. If a back-up breaker is used rather than fuses, the fuse voltages are all set to zero.

3. Fault arc characteristics

The single-phase high-current arc in air has a rising *V-I* characteristic which can be represented as

$$V_{ARC} = V_E + k\, I_{ARC}{}^X g^Y \qquad (2)$$

Measurements by Fisher [10] using currents up to 41.6kA and arcing gaps *g* from 25-100mm found that $X \approx 0.15$ and $Y \approx 0.5$. Ignatko [11] studied arcs from 5-150kA with gaps from 5-200mm. He measured the electrode-fall voltage (V_E) with Langmuir probes (23.5V for copper electrodes), and the actual arc length (which is greater than the gap distance) was measured photographically, to obtain the column gradient. Ignatko's data also fits the form of equation (2), with similar *X* and *Y* to Fisher's.

Stokes and Oppenlander [12] found $X \approx 0.12$ and $Y \approx 1.0$ for horizontal and vertical gaps of 5-500mm with currents up to 20kA. Their photographs revealed the complex variations in arc geometry in detail. Paukert [13] reviewed data from seven different laboratories and found approximate average values of $X \approx 0.2$ and $Y \approx 0.47$.

Given the very variable nature of the fault arc the data in the literature shows a remarkable agreement. The arc voltage shows a weakly rising dependence on current, with $X \approx 0.12$-0.2. In some cases it is not clear whether published data refers to instantaneous current or true r.m.s. current, but the trend is the same. The dependence on *g* is more variable, probably as a result of the use of differing electrode geometries.

For the 3-phase case, the behaviour of the arcing fireball is different and not well known, but as a first step (as originally suggested by Fisher) it can be represented as 3 separate star-connected single-phase arcs, each of which can be modelled by an equation of the same form as (2), but the values of *k, X* and *Y* have not been measured directly.

The unknown 3-phase values of *X* and *Y* were determined using the following procedure. First the value of a constant arc voltage was found which gave a true r.m.s. arcing current which agreed exactly with the values measured in the IEEE tests. This was done by repeatedly solving (1) for each test shot, computing the true r.m.s. current over the last cycle before the circuit opened, and iteratively adjusting V_{ARC} to obtain agreement. Then *X* and *Y* were determined by multiple regression (304 test shots were used in the analysis). This gave $X = 0.173$ and $Y = 0.222$, values which are consistent with expectations from data on the single-phase arc.

Then it was assumed that the same *X* and *Y* can be used to relate the instantaneous arc voltage and current (*v* and *i*), giving a nonlinear transient arc model of the form

$$v_{ARC} = V_E + K\, i_{ARC}{}^{0.173} g^{0.222} \qquad (3)$$

Finally the value of *K* was found by a second iterative fitting to the measured arcing current. However *K* was not constant, but a relatively strong function of the line-to-line test voltage V_{LL}. ($K = 1.827 V_{LL}{}^{-0.377}$ with V_{LL} in kV). This dependency is not easy to explain, but can also be found in Schau and Schade [14] and the IEEE formula. It is probably connected with the assumption that the arc is quasi-static, and possibly that the effects of arc extinction and restriking around voltage zero are not modelled. There was also a box effect; *K* must be multiplied by 0.797 for tests in a box.

Using this model together with the circuit equations (1), the circuit currents, voltages, power

and energy can be computed. Typical results are shown in Figs. 3a-3d for an ungrounded arcing fault.

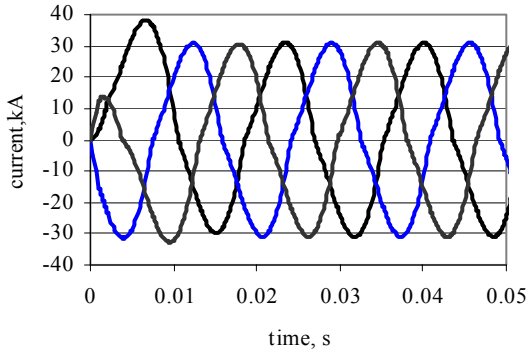

Fig. 3a: Computed current transients

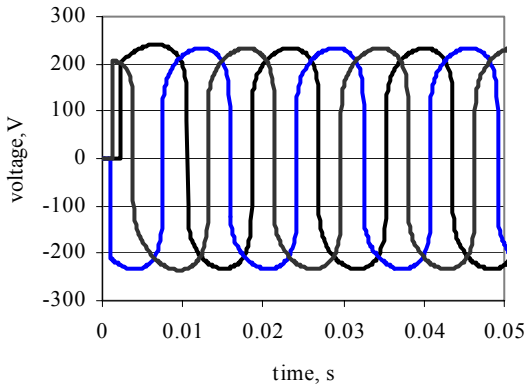

Fig. 3b: Computed arc voltage transients

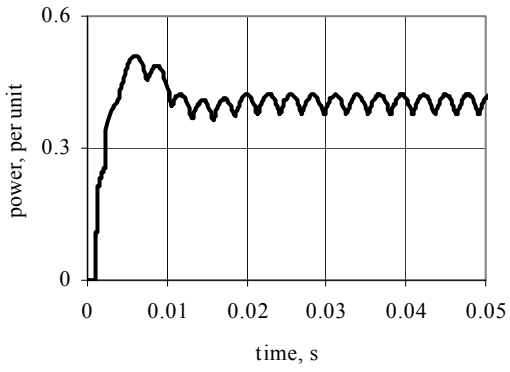

Fig. 3c: Instantaneous 3-phase power

The waveshapes are similar to published data [5,14]. The current stabilises quite quickly because of the damping effect of the fault arc resistance. The delay in appearance of the arc voltage is the fusion time of the fine trigger wires in each phase. Fig. 3c shows the instantaneous power as a fraction of the bolted-fault VA. In the example shown this ratio is close to the worst-case value of 0.5. The build-up of arc energy in Fig. 3d is almost linear, but with a delay of a few milliseconds after the fault begins.

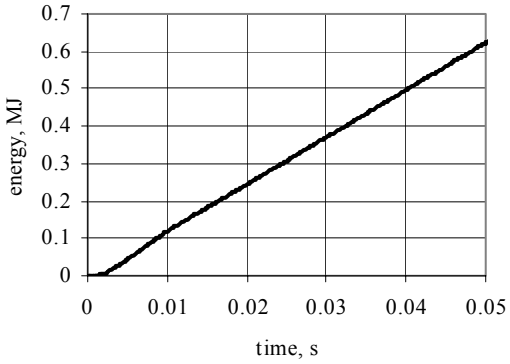

Fig. 3d: Total arc energy

These solutions were obtained using 4th order Runge-Kutta integration of the equations, with automatic adjustment of the time step to achieve a preset accuracy. However the resistance of the arc model (3) tends to infinity as the current nears zero, giving a very low circuit time-constant, which causes the time step to be reduced to a very small value, and the solution "grinds to a halt". The method of solving this problem is given in section 8.

Gammon and Matthews [15] calculated arcing currents for 1-phase arcing faults using a similar time-domain method (Runge-Kutta integration, using both Fisher's and Stokes and Oppenlander's model). They assumed that the arc extinguishes at each current zero and then reignites in the next half-cycle when the gap voltage reaches a fixed breakdown level (dielectric reignition), whereas the model described here shows a continuous variation of current through the zero-crossing period. Dielectric reignition occurs for a 1-phase arc where the power input to the arc drops to zero when the current reaches zero. However for a 3-phase arcing fireball the situation is less clear. Although the current in one phase may reach zero the power input to the fireball continues via the other two phases.

3.1 Calculation of arcing current

Using the model the r.m.s. arcing current (geometric mean value for the 3 phases over the last cycle before circuit opening) was computed and compared with the measured values given in [8]. The results are shown in Fig. 4a, and the values predicted by the IEEE formula are shown in Fig 4b.

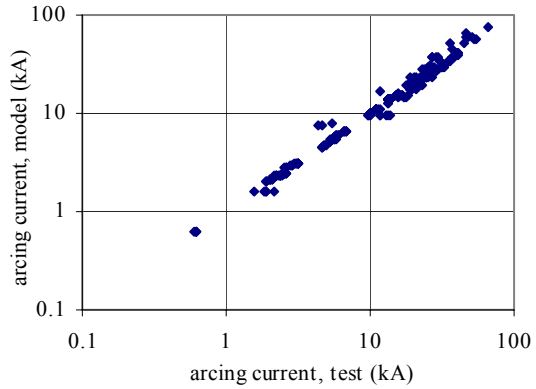

Fig. 4a: Comparison of predicted and measured arcing current (time-domain model).

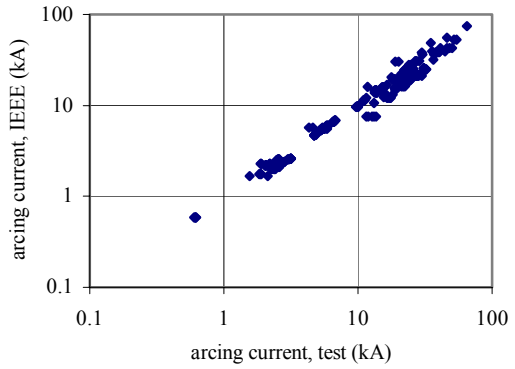

Fig. 4b: Comparison of predicted and measured arcing current (IEEE 1584 model).

The time-domain model gives a slightly better correlation (r^2=0.989) than the IEEE formula (r^2=0.978). The computed value of total arc energy also agreed well with the test values (r^2=0.955).

Fuses were not used for the tests shown in Fig. 4, the circuit being cleared by a back-up breaker. The data covers voltages from 208V to 13.8kV, bolted fault currents from 700A to 106kA, arcing gaps from 7.1mm to 152mm, and various box dimensions, as well as tests in the open (304 tests in all).

4. Calculation of incident energy density

In [8] it is assumed that the incident energy density falls with distance from the arcing fireball according to ($1/d^x$) where x is a "distance exponent". For a spherical fireball in the open with a total energy W_{ARC} the direct radiated energy density at a distance d is $\beta W_{ARC}/(4\pi d^2)$ where β is the fraction of the total arc energy which is emitted as radiant heat. The distance exponent in this case is 2.

For tests in an open box, the focusing effect of the box changes the situation, as shown in Fig. 5.

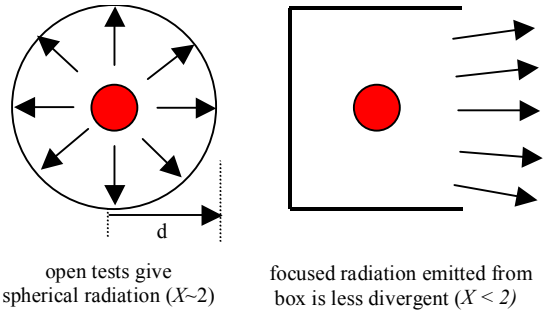

Fig. 5: Box focusing effect

For open box tests, as d gets smaller, the distance exponent falls, eventually towards zero, when the radiant heat appears as a plane wave. The same effect can occur as the box dimensions change. Reflections of heat from the back and sides of the box can make the arc and the box appear as one much larger heat source, reducing the effective distance exponent.

4.1 Tests in the open

Fitting to the IEEE test data using multiple regression gave the following model :

$$E_{max} = 0.1026\, E_S^{0.958}\, g^{0.284}\, V_{LL}^{-0.532} \quad (4)$$

E_{max} = mean maximum energy density at a distance d, (cal/cm^2)
E_S = spherical component of energy density = $W_{ARC}/(4\pi\, d^2)$
W_{ARC} = total computed arc energy , J

Fig. 6 shows a good correlation (r^2 = 0.949) between the predictions of (4) and the test values.

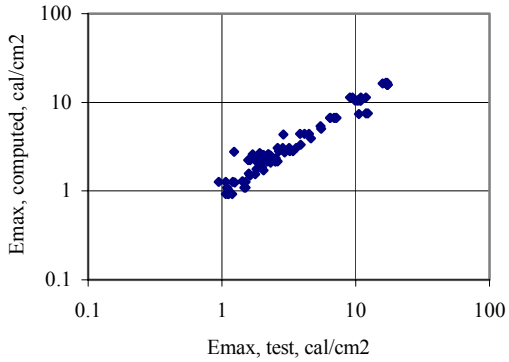

Fig. 6: Predicted incident energy, all open tests

4.2 Tests in a box with one side open

Rather than using distance exponents, it is possible to calculate the focusing effect of the box directly, using **radiative view factors** [16]. The view factor *Fij* between 2 surfaces *i* and *j* is defined as the fraction of the radiated energy leaving surface *i* which strikes surface *j*.

Radiated energy from the arc strikes the back and sides of the box and is then reflected out towards the calorimeters. It is necessary to take multiple reflections into account, as these are not negligible. The inner surfaces behave as **diffuse absorbers and reflectors** with a reflectivity α. Incident radiation is reflected equally in all directions, as illustrated in Fig.7.

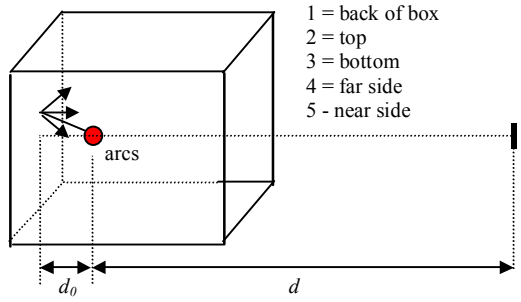

Fig. 7: Box geometry for calculation of reflections

The arcing fireball is treated as a spherical source of heat. For a single reflection the fraction of the arc energy which strikes side *k* is $F_{SK}.(\beta\, W_{ARC})$. F_{SK} is the view factor from a spherical heat source to a rectangular plate, and is an easily calculated geometrical function [16]. If the diffuse reflectivity is α, the fraction of the reflected energy which strikes the calorimeter is then $\alpha.F_{SK}.F_{KC}\,(\beta.W_{ARC})$, where F_{KC} is the view factor between side *k* and the calorimeter. Using the reciprocity principle [16] $A_C F_{CK} = A_K F_{KC}$, where A_K is the area of side *k* and A_C is the area of the calorimeter. So the energy striking the calorimeter is $\alpha.F_{SK}.F_{CK}\,(A_C/A_K)\,(\beta W_{ARC})$. This then gives the incident energy density at the calorimeter due to a single reflection as

$$E_1 = \alpha.F_{SK}.(F_{CK}/A_K)\,(\beta W_{ARC})$$

where F_{CK} is the view factor from the calorimeter to the side *k*.

Multiple reflections are treated similarly. For a triple reflection, say from the arc to the back of the box (side 1), then to the far side (4), then to the bottom (3), the energy arriving at the calorimeter is

$$E_3 = \alpha^3.F_{S1}.F_{14}.F_{43}.\,(F_{C4}/A_4)\,(\beta.W_{ARC})$$

and the total reflected energy $F_R(\alpha).W_{ARC}$ is obtained by summing all the contributions from all the reflections. For a 5-sided box the number of possible reflections off *N* surfaces is *5!/(5-N)!* a total of 325 paths, as shown below.

No of reflections	No of paths
1 (i.e. single)	5
2	20
3	60
4	120
5	120

Although there are a large number of quadruple and quintuple reflection paths, their contribution to the total energy is small because of the multiplying factor α^4 or α^5, and the reflectivity α must be less than 1. Using this method the effect of the box can be taken into account simply by adding the total reflected energy density to the spherical component (which strikes the calorimeter directly without any reflections). Eqn (4) is then modified to

$$E_{\max} = 0.1026\{E_S + F_R(\alpha)W_{ARC}\}^{0.958} g^{0.284} V_{LL}^{-0.532} \quad (5)$$

The only unknown is the reflectivity α. By varying α and computing the correlation between the predictions of (5) and the test data, the optimum value of α was found to be 0.56. This corresponds well with values to be expected from graybody diffuse reflectors. In a typical case direct spherical radiation accounts for about 50% of the incident energy while the paths with 5 reflections contribute only 0.1%. Multiple reflections of higher order than this can be neglected.

Fig. 8a shows a comparison between the incident energy density predicted by (5) and the measured mean maximum values for the entire IEEE data set.

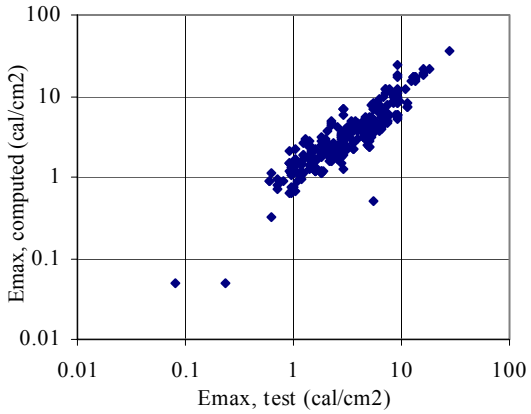

Fig. 8a: Computed vs. measured incident energy

Fig. 8b gives a similar comparison for the IEEE formula.

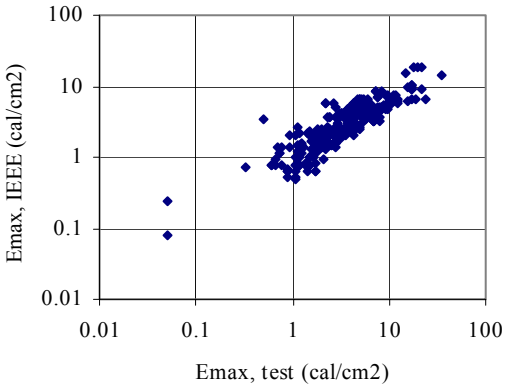

Fig. 8b: IEEE formula prediction compared with test

The time-domain computer model gives a significantly better correlation ($r^2 = 0.856$) than the IEEE formula ($r^2 = 0.775$). While the chief cause of variability is the chaotic behaviour of the fault arc, it is also clear that variations in reflectivity of the inner box surfaces will make a significant difference to the results.

5. Effect of current-limiting fuses

The model used is based on that described in [17], with some enhancements.

5.1 Prearcing model

The melting time is found by computing the evolution of the true r.m.s. current in each phase, and switching to the arcing state when the fuse's melting-time/current characteristic is crossed, as shown in Fig. 9.

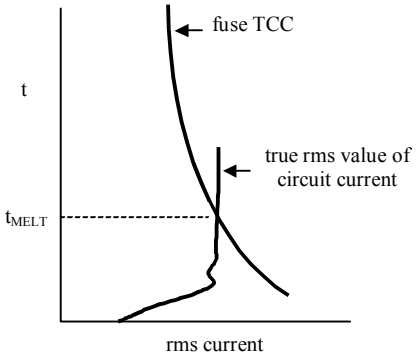

Fig.9: Computation of melting time

The fuse TCC is stored as a table which is dynamically fitted with cubic spline functions, and interpolation is used (as with all the models), to find the exact crossing point. For times shorter than the lowest tabulated value, the adiabatic melt I^2t is used.

The true r.m.s. (virtual) current in each phase is computed as $[\int i^2 dt / t]^{0.5}$

5.2 Arcing models

These are as given in [17] and model arc ignition in the notches, burnback, fusion of the sand, arc merging, and final arc extinction. Each arc is modelled as a simple cylindrical channel. For each fuse design, details of the element construction and materials are needed, and the resulting models give very good agreement with oscillograms obtained from fuse type testing.

Figs. 10a-10c show the results of typical calculations for the interruption of a 50kA ungrounded arcing fault in a 600V 60Hz 3-phase system by an 800A class L fuses, closing at zero degrees of phase *a*. The other data used to obtain these results was :

p.f. = 0.1 g = 32 mm
d_0 = 102 mm d = 457.2 mm
and the box size was 508 x 508 x 508 mm.

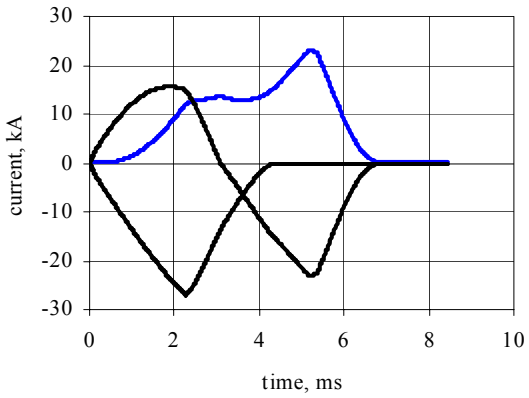

Fig.10a: Currents for arcing fault with fuses

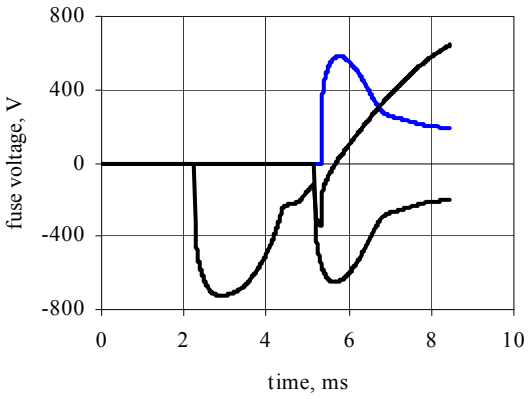

Fig. 10b: Fuse arc voltages

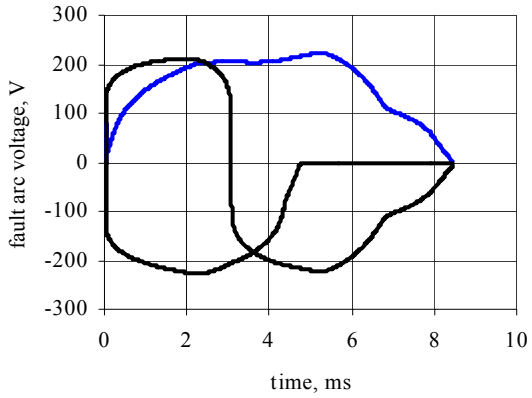

Fig. 10c: Arcing fault voltages

In the case shown the fuse in phase *c* melts first and limits the current. The appearance of the phase *c* fuse arc voltage changes the rates-of rise of current in the other two phases. The phase *b* and phase *a* fuses melt just before the phase *c* fuse clears, and then the *b* and *a* fuses clear together against the line-to-line voltage.

5.3 Point-on-wave effects

The possible sequences of events during clearing are very complicated, involving fuse melting and clearing in each phase, merging of arcs between notches, and interaction between the phases (if the fault is ungrounded). If a fuse just fails to melt within a particular half-cycle, the melting time jumps to a subsequent half-cycle. In Figs. 10 all 3 fuses opened, but in many cases only 2 fuses operate.

The results are also affected by the point-on-wave at which the arcing fault begins. For 3-phase systems, all possible outcomes are covered if the closing angle θ (with respect to the voltage of phase *a*) is varied in the range $0 \le \theta \le 60°$.

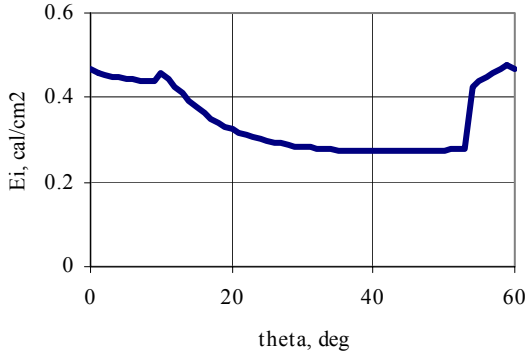

Fig. 11a: 3x1200A class L fuses @ 100kA

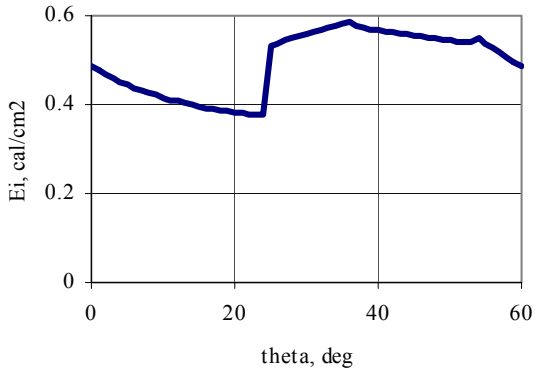

Fig. 11b: 3x1200A class L fuses @ 44.7kA

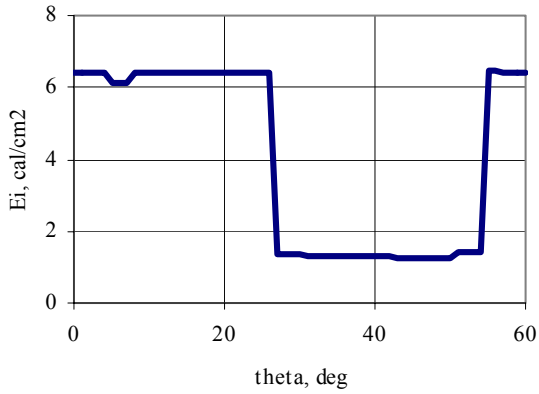

Fig. 11c: 3x1200A class L fuses @ 18.25 kA

Figs. 11a - 11c show the variation of arc flash energy density E_i with closing angle for three levels of bolted fault current. There are many discontinuities, associated with different sequences of fuse operation. Near the threshold current (Fig. 11c), the jumps in E_i are very large.

Fig. 12 shows the computed critical closing angle (i.e. that which produces the highest value of E_i) for a 1600A class L fuse, as a function of available bolted fault current.

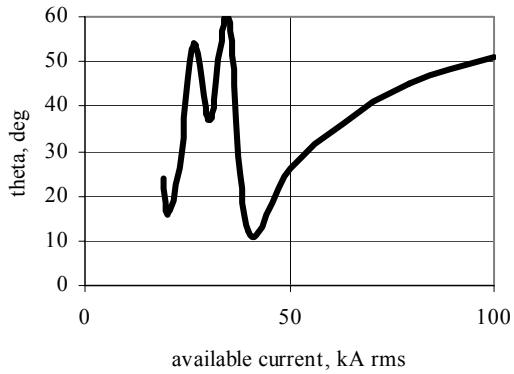

Fig. 12: Critical closing angle, 1600A class L fuses

Below the threshold (about 20kA for Fig. 12) the results are not significantly affected by closing angle. Within the threshold region (20-40kA for Fig. 12) the critical angle oscillates wildly as the available current is changed. Above the threshold (in the current-limiting region) the curve becomes smooth but does not always increase as shown. For some fuses a discontinuity followed by a decrease can be observed.

After examining point-on-wave effects for several different fuse designs, and considering the additional variations which will be found in practice, due to the chaotic fault arc behaviour, it is concluded that it is not possible to recommend a worst-case closing angle for arc-flash testing, in a similar way to that which is used for type testing of current-limiting fuses. The best recommendation appears to be to use random closing, but with several tests, to obtain a range of arc flash energy values.

5.4 Arc flash characteristic

For a given set of data (equipment type and circuit parameters) it is useful to plot the arc flash energy density as a function of available current. Fig. 13 shows a typical characteristic computed for a set of 3 1200A class L fuses. The upper curve is the maximum value (worst closing angle) and the lower curve is the minimum value (best closing angle).

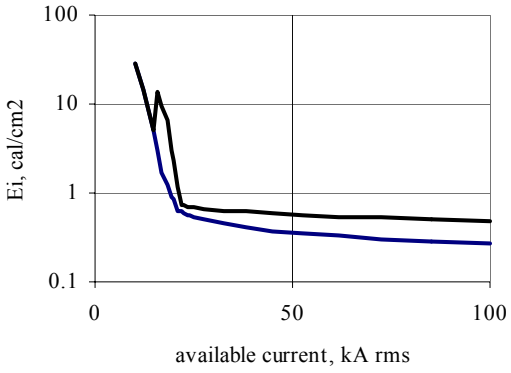

Fig. 13: Arc flash characteristic

Fig. 13 is similar to published test data [18] for 1200A class L fuses, although for slightly different test conditions. It shows that this fuse can limit the arc flash energy density to a level well below the critical value for a 2nd-degree burn (1.2 cal/cm^2), but only if the available bolted-fault current is high enough to cause operation in the current-limiting mode.

For these calculations it was assumed that the fault arcs were represented by (3) with unchanged values of *k, X* and *Y*. However, some changes may be needed, because Stokes and Oppenlander [12] showed that for time durations of a few milliseconds, the arc does not move far from its starting location, so the fault arc geometry for very short times will be different from that which develops over a period of several cycles, giving a possibly significant change in fault arc voltage and incident energy.

6. Conclusions

A time-domain model of arc flash hazard has been developed. The ordinary differential equations for the 3-phase circuit and any current-limiting fuses are solved by 4th-order RK integration with automatic control of the time step.

The arcing fault fireball is represented as a star-connected set of non-linear resistors, and the their characteristics have been determined by least-squares fitting to the published IEEE dataset. The resulting arc characteristics are similar to those which have previously been measured for high-current single-phase arcs in air.

For arcing faults in an open box, the focusing effect of the box is taken into account using radiation view factors to allow for multiple reflections of radiant heat.

The final model calculates the incident energy density due to the arc flash at a distance *d* for tests in the open or in a box of arbitrary dimensions, with a given electrical power system and interbus electrode gap. It gives good correlation with the IEEE 1584 test data and can also be used to study point-on-wave and other effects.

Furthermore the model has the potential for further improvement if a better model of the arcing fireball can be developed.

7. References

[1] National Electric Code, 2002 Edition. National Fire Protection Association. NFPA 70.

[2] Standard for Electrical Safety Requirements for Employee Workplaces, NFPA 70E, 2003 Edition. National Fire Protection Association.

[3] Jones, R.A, and 9 other members of an IEEE-PCIC working group. "Staged Tests Increase Awareness of Arc-Flash Hazards in Electrical Equipment". IEEE Petroleum and Chemical Industry Conference Record, Sept 1997, pp 313-332.

[4] Lee, R.H. "The Other Electrical Hazard: Electric Arc Blast Burns". IEEE Transactions on Industry Applications, vol IA-18. No 3, May-June 1982, pp 246-251.

[5] Neal, T.E., Bingham, A.H. and Doughty, R.L. "Protective Clothing Guidelines for Electric Arc Exposure". IEEE

Transactions on Industry Applications, vol 33, No 4, July/August 1997, pp 1043-1054.

[6] Doughty, R.L., Neal, T.E., and Floyd II, H.L. "Predicting Incident Energy to better manage the Electric Arc Hazard on 600V distribution systems". Proc.IEEE PCIC, Sept 1998, pp 329-346.

[7] Doughty, R.L., Neal, T.E., Dear, T.A. and Bingham, A.H. "Testing Update on Protective Clothing and Equipment for Electric Arc Exposure", IEEE Industry Applications Magazine, Jan-Feb 1999, pp 37-49.

[8] IEEE Guide for Performing Arc-Flash Hazard Calculations. IEEE Standard 1584, IEEE, September 2002.

[9] Wilkins, R. "3-phase operation of current-limiting power fuses", 3rd Int Conf on Electric Fuses and their Applications, Eindhoven, 1987, pp 137-141.

[10] Fisher, L.E. "Resistance of low-voltage arcs". IEEE Transactions on Industry and General Applications, vol IGA-6, No 6, Nov-Dec 1970, pp 607-616.

[11] Ignatko, V.P. "Electric characteristics of AC open heavy-current arcs". 3rd International Symposium on Switching Arc Phenomena, TU Lodz, Poland, 1977, pp 98-102.

[12] Stokes, A.D. and Oppenlander, W.T. "Electric arcs in open air". J. Phys. D: Appl. Phys. vol 24, 1991, pp26-35.

[13] Paukert, J. "The arc voltage and the resistance of LV fault arcs". 7th International Symposium on Switching Arc Phenomena, TU Lodz, Poland, 1993, pp 49-51.

[14] Schau, H. and Stade, D. "Requirements to be met by protection and switching devices from the arcing protection point of view". Proceeding of 5th International Conference on Electric Fuses and their Applications, Technical University of Ilmenau, Germany, Sept 1995, pp 15-22.

[15] Gammon, T. and Matthews, J. "Instantaneous arcing-fault models developed for building system analysis". IEEE Transactions on Industry Applications, vol 37, No 1, 2001, pp197-203.

[16] Ozisik, M.N. "Heat Transfer", McGraw-Hill, 1985.

[17] Wilkins, R. "Standard Fuse Model for System Short-Circuit Studies." 8th International Symposium on Switching Arc Phenomena, TU Lodz, Poland, 1997, pp 163-166.

[18] Doughty, R.L., Neal, T.E., Macalady, T.L., and Saporita, V. "The use of Low-Voltage Current-Limiting Fuses to Reduce Arc Flash Energy." IEEE Transaction on Industry Applications, vol 36, no 6, November-December 2000, pp 1741-1749.

8. Appendix

The numerical problem associated with the infinite fault arc resistance as the current passes through zero can be solved by connecting a fictitious high-value shunt resistor in parallel with the fault arc as shown below.

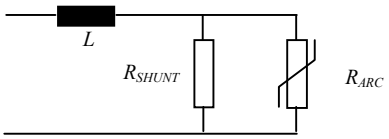

Before solution R_{SHUNT} is set to *L/1.0E-6* which ensures that the series time constant never falls below 1μs, whatever the value of R_{ARC}. This produces a smooth and rapid progression of the solution through the current zero. Furthermore the value of R_{SHUNT} is so high that it makes a negligible difference to the r.m.s. arcing current, I^2t and energy. However there is a penalty to pay for this. During the solution it is essential to calculate how the total circuit current divides between the two parallel resistors, to avoid numerical instability, and so that the arc voltage can be calculated. This is not trivial, as R_{ARC} is non-linear. However it can be done simple and quickly using the Newton-Raphson method. Without this computational device the model and solution method described in section 2 could not be implemented.